This is a repository copy of *Decoupled spin dynamics in the rare-earth orthoferrite YbFeO3: Evolution of magnetic excitations through the spin-reorientation transition*.

White Rose Research Online URL for this paper:
http://eprints.whiterose.ac.uk/167065/

Version: Published Version

eprints@whiterose.ac.uk
https://eprints.whiterose.ac.uk/

Decoupled spin dynamics in the rare-earth orthoferrite YbFeO₃:
Evolution of magnetic excitations through the spin-reorientation transition

S. E. Nikitin,[1,2] L. S. Wu,[3] A. S. Sefat,[4] K. A. Shaykhutdinov,[5] Z. Lu,[6] S. Meng,[6,7] E. V. Pomjakushina,[8] K. Conder,[8]
G. Ehlers,[9] M. D. Lumsden,[3] A. I. Kolesnikov,[3] S. Barilo,[10] S. A. Guretskii,[10] D. S. Inosov,[2] and A. Podlesnyak[3,*]

[1]*Max Planck Institute for Chemical Physics of Solids, Nöthnitzer Str. 40, D-01187 Dresden, Germany*
[2]*Institut für Festkörper- und Materialphysik, Technische Universität Dresden, D-01069 Dresden, Germany*
[3]*Neutron Scattering Division, Oak Ridge National Laboratory, Oak Ridge, Tennessee 37831, USA*
[4]*Materials Science and Technology Division, Oak Ridge National Laboratory, Oak Ridge, Tennessee 37831, USA*
[5]*Kirensky Institute of Physics, Federal Research Center, Krasnoyarsk 660036, Russia*
[6]*Helmholtz-Zentrum Berlin für Materialien und Energie, D-14109 Berlin, Germany*
[7]*China Institute of Atomic Energy, Beijing 102413, People's Republic of China*
[8]*Laboratory for Multiscale Materials Experiments, Paul Scherrer Institut, CH-5232 Villigen PSI, Switzerland*
[9]*Neutron Technologies Division, Oak Ridge National Laboratory, Oak Ridge, Tennessee 37831, USA*
[10]*Institute of Solid State and Semiconductor Physics, National Academy of Sciences, 220072 Minsk, Belarus*

In this paper, we present a comprehensive study of magnetic dynamics in the rare-earth orthoferrite YbFeO₃ at temperatures below and above the spin-reorientation (SR) transition $T_{SR} = 7.6$ K, in magnetic fields applied along the a, b, and c axes. Using single-crystal inelastic neutron scattering, we observed that the spectrum of magnetic excitations consists of two collective modes well separated in energy: 3D gapped magnons with a bandwidth of ~60 meV, associated with the antiferromagnetically (AFM) ordered Fe subsystem, and quasi-1D AFM fluctuations of ~1 meV within the Yb subsystem, with no hybridization of those modes. The spin dynamics of the Fe subsystem changes very little through the SR transition and could be well described in the frame of semiclassical linear spin-wave theory. On the other hand, the rotation of the net moment of the Fe subsystem at T_{SR} drastically changes the excitation spectrum of the Yb subsystem, inducing the transition between two regimes with magnon and spinonlike fluctuations. At $T < T_{SR}$, the Yb spin chains have a well defined field-induced ferromagnetic (FM) ground state, and the spectrum consists of a sharp single-magnon mode, a two-magnon bound state, and a two-magnon continuum, whereas at $T > T_{SR}$ only a gapped broad spinonlike continuum dominates the spectrum. In this work we show that a weak quasi-1D coupling within the Yb subsystem J_{Yb-Yb}, mainly neglected in previous studies, creates unusual quantum spin dynamics on the low-energy scales. The results of our work may stimulate further experimental search for similar compounds with several magnetic subsystems and energy scales, where low-energy fluctuations and underlying physics could be "hidden" by a dominating interaction.

I. INTRODUCTION

Quantum phase transitions have been a matter of special interest in condensed matter physics during the last decades [1–3]. In contrast to the classical phase transitions induced by thermal fluctuations, quantum phase transitions are driven by quantum fluctuations and can be induced by an external tuning parameter, like pressure, magnetic field, uniaxial strain, etc. Among all quantum critical systems, the antiferromagnetic (AFM) Heisenberg $S = 1/2$ chain is one of the simplest examples: at zero field it has a tangled singlet ground state and fractionalized magnetic excitations, the so-called "spinons" carrying spin 1/2 [4,5], whereas in a magnetic field it undergoes a transition into the field-polarized state, with a well defined classical FM ground state and $S = 1$ magnon quasiparticles as elementary excitations [6]. In this work, we studied the spin

dynamics of YbFeO₃, which contains two magnetic sublattices and observed an intriguing coexistence of the classical high-energy spin waves and unconventional low-energy spin excitations, which spontaneously transform from classical magnon to quantum spinon quasiparticles with increasing temperature.

YbFeO₃ belongs to the family of iron-based orthorhombic perovskites, RFeO₃ (R is a rare-earth element, Bi, or Y), which attract considerable attention due to the high-temperature multiferroic properties of BiFeO₃ [7,8], anisotropic magnetic entropy evolution [9], laser-pulse induced ultrafast spin-reorientation [10–12], etc. Magnetic property investigations of the rare-earth orthoferrites RFeO₃ have shown that the Fe³⁺ moments ($S = 5/2$) are ordered in a canted AFM structure Γ4 at high temperature with $T_N \approx 600$ K (details of the notations are given in Ref. [13]), and the spin canting gives a weak net ferromagnetic moment along the c axis [Fig. 1(c)] [13–15]. Furthermore, symmetry analysis and careful neutron diffraction measurements have found a second "hidden" canting along the b axis, which is symmetric relative to the ac plane and does
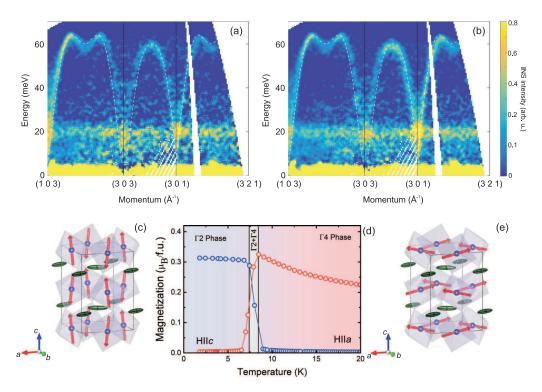
FIG. 1. [(a) and (b)] Magnon excitations in YbFeO$_3$ along (103)-(303)-(301)-(321) directions of reciprocal space taken at temperatures below ($T = 2$ K, left) and above ($T = 15$ K, right) the SR transition (indices are given in reciprocal lattice units). Dotted lines represent results of the linear spin-wave calculations. [(c) and (e)] Sketches of magnetic structures of YbFeO$_3$ below (c) and above (e) the SR transition. Blue spheres show Fe ions, green ellipsoids represent anisotropic magnetic moments of Yb. In the magnetic phase $\Gamma2$ (c), below T_{SR}, Fe moments align along the c axis, and spin canting results in a net moment along the a axis. Above T_{SR} ($\Gamma4$ phase), Fe moments rotate to the a axis, and spin canting gives a net moment along the c axis. (d) Temperature dependencies of the magnetization of YbFeO$_3$ measured at $H = 0.01$ T along the c (red) and a (blue) axes.

not create a net moment [16,17]. With decreasing temperature, a spontaneous spin-reorientation (SR) transition from $\Gamma4$ to the $\Gamma2$ magnetic configuration occurs in many orthoferrites with magnetic R ions [13,14] in a wide temperature range from $T_{SR} \approx 450$ K for SmFeO$_3$ down to $T_{SR} \approx 7.6$ K for YbFeO$_3$, and the net magnetic moment rotates from the a to the c axis [see Figs. 1(c)–1(e)]. Most of previous work that was devoted to the investigation of the SR transition in RFeO$_3$, associated this phenomenon with the R-Fe exchange interaction, because orthoferrites with nonmagnetic $R = $ La, Y, or Lu preserve the $\Gamma4$ magnetic structure down to the lowest temperatures.

Taking into account three characteristic temperatures: $T_N^{Fe} \sim 600$ K, $T_{SR} \sim 10$ K, and $T_N^{Yb} \sim 1$ K (known for the isostructural YbAlO$_3$ [18]), one could expect a similar hierarchy of the exchange interactions $J_{Fe\text{-}Fe} \gg J_{Fe\text{-}Yb} \gg J_{Yb\text{-}Yb}$ and multiple magnetic modes, corresponding to each of the energy scales. From the experimental point of view, the best experimental technique to study the details of the magnetic interaction is the inelastic neutron scattering. However, to the best of our knowledge, investigations of the spin dynamics in the orthoferrites were mainly focused on the Fe subsystem. Results of the INS experiments have shown that the Fe spin fluctuations are dominated by the high-energy gapped magnons with an energy scale of $E \approx 60$ meV and could be reasonably well described using a simple linear spin-wave theory (LSWT) [19–22], while the details regarding the dispersion of magnetic

modes, associated with R-Fe and R-R exchange interactions, were mainly unexplored.

In this paper, we present the results of a detailed study of the spin dynamics in YbFeO$_3$ that covers the energy scales mentioned above. We observed the high-energy spin-wave modes within the Fe-subsystem at $E \approx 4$–65 meV, which are almost unaffected by the SR transition. Well below the gap of the Fe excitations $\Delta \approx 4$ meV, we observed a second gapped excitation, with dispersion along the c axis only, which can be associated with the fluctuations of the Yb moments coupled in quasi-1D XXZ spin chains. The most remarkable outcome of our work is an unusual low-dimensional spin dynamics of the highly anisotropic Yb subsystem, which significantly changes through the SR transition. Below T_{SR}, Yb moments are fully polarized by the effective Fe field, giving rise to the conventional magnons accompanied by a higher-energy 2-magnon bound state and a broad continuum. On the other hand, above T_{SR}, an effective field is transverse to the easy axis, leading to the nonpolarized ground state and to the rise of unconventional spinon excitations, which are clearly seen as a broad continuum above the single-particle mode in the excitation spectrum. INS measurements of low-energy spin dynamics under magnetic field along different axes show that the external magnetic field has a similar effect as the effective internal field, induced by the Fe subsystem.

II. EXPERIMENTAL DETAILS

INS experiments were carried out on two YbFeO$_3$ single crystals with the masses of ~ 3.8 g [used in time-of-flight (TOF) measurements on the SEQUOIA and CNCS instruments] and ~ 1.2 g [for measurements on the triple-axis spectrometer (TAS) FLEXX] with a mosaicity $\leq 1°$. The crystals were grown by the floating-zone method and using the fluxed melt crystallization (on seeds) technique, respectively (see Refs. [23,24] for details). Most of the INS measurements were performed using TOF spectrometers: Cold Neutron Chopper Spectrometer (CNCS) [25,26] and SEQUOIA [27] at the Spallation Neutron Source (SNS) at Oak Ridge National Laboratory. For the high-energy measurements on the SEQUOIA instrument, we fixed the incident neutron energy $E_i = 100$ meV and oriented the sample with the [010] direction vertically. Data were taken at temperatures above ($T = 15$ K) and below ($T = 2$ K) the SR transition. For the low-energy measurements, we used the CNCS instrument. The sample was measured in two orientations, with either [100] or [010] directions pointed vertically, and the vertical magnetic field was applied along the a and b axes, respectively. The measurements were carried out using the rotating single crystal method at temperatures of $T = 2$ and 10 K. The data were collected using a fixed incident neutron energy of $E_i = 3.0$ meV resulting in a full-width at half-maximum energy resolution of 0.07 meV at the elastic position.

All time-of-flight data sets were combined to produce a four-dimensional scattering-intensity function $I(\mathbf{Q}, \hbar\omega)$, where $\mathbf{Q}$ is the momentum transfer and $\hbar\omega$ is the energy transfer. For data reduction and analysis we used the MANTID [28], HORACE [29], and SPINW [30] software packages. For the crystal electric field (CEF) calculations and numerical diagonalization of the 1D-XXZ Hamiltonian, we used MCPHASE [31] and ALPS [32,33] software, respectively.

Low-energy INS measurements with horizontal magnetic field applied along the c axis were performed using the cold-neutron triple-axis spectrometer FLEXX (V2) [34] with the HM-1 magnet at the Helmholtz-Zentrum Berlin (HZB). The sample was mounted and mechanically fixed in a special aluminum container in order to avoid magnetic field-induced torque due to a strong anisotropy of magnetization of YbFeO$_3$ at low temperatures. Measurements were carried out with a fixed final energy ($k_f = 1.3$ Å^{-1}) at temperatures between 2 and 10 K and magnetic fields up to $H = 4$ T.

Specific-heat measurements were carried out using a commercial PPMS-6000 from Quantum Design in magnetic fields up to 12 T applied along the a axis. Magnetization curves were measured using a vibrating-sample magnetometer MPMS-3 with a magnetic field up to 7 T applied along the a and c axes.

III. ZERO-FIELD MEASUREMENTS: EXPERIMENTAL RESULTS

A. High-energy INS data

The spin dynamics of the Fe subsystem of rare-earth orthoferrites with various rare-earth ions ($R =$ Lu, Y, Tm, Er) were a matter of comprehensive investigations [19–22]. However, to the best of our knowledge, the details of spin dynamics of YbFeO$_3$ have not been published yet and we
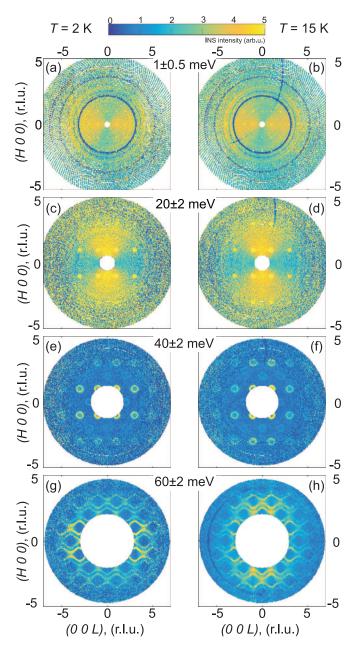

FIG. 2. Constant energy slices of the INS intensity within the ($H0L$) scattering plane taken at [(a), (c), (e), and (g)] $T = 2$ and [(b), (d), (f), and (h)] 15 K. The scattering intensities were integrated within the energy windows indicated between the corresponding panels. The intensities of (a) and (b) have been scaled $\times 0.1$ due to the proximity of the elastic line.

start the discussion of our INS data with the report of the high-energy spin dynamics. Figures 1(a) and 1(b) presents experimental INS spectra along all principal Q_H, Q_K, and Q_L directions, taken at temperatures $T = 2$ and 15 K, below and above the SR transition, respectively. Observed magnon branches stem from the magnetic Bragg peaks with an even sum of $H + K + L$, and the maximum energy of spin-wave branches $E_{max} \approx 65$ meV is similar to that observed in other orthoferrites and could be clearly associated with a collective excitation of the Fe^{3+} magnetic moments. The horizontal dispersionless line at $E \approx 20$ meV was associated with the
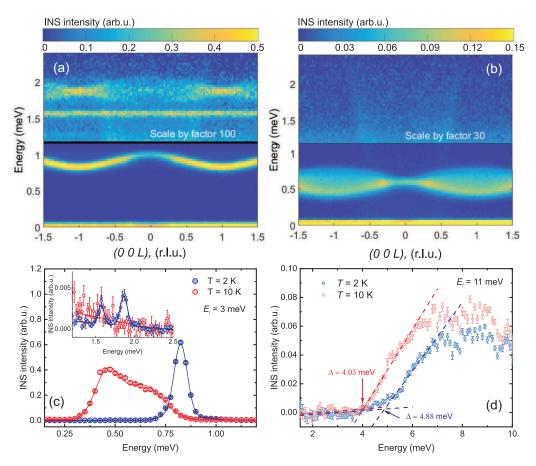
FIG. 3. Low-energy excitation spectra of YbFeO$_3$ at (a) $T = 2$ (a) and (b) 0 K (b) taken at CNCS. Energy slices are taken along the $(00L)$ direction with $(0K0)$ and $(H00)$ integrated over the range $[-0.5, 0.5]$. The intensity of the upper part of the panels has been scaled $\times 100$ and $\times 30$ to make two-kink excitations visible. The shadow in the center is due to direct beam. (c) Energy cuts through the (001) direction taken for the both temperatures. Solid lines show results of fitting with one and two Gaussians for $T = 2$ and 10 K, respectively. The intensity of the $T = 10$ K spectrum was scaled with a factor of 3. (Inset) Zoom of the energy cut at $[1.2, 2.5]$ meV range, showing two-kink excitations at 2 K. (d) Energy cuts at $\mathbf{Q} = (101)$, taken at $T = 2$ and 10 K to show the gap in the excitation spectrum of Fe^{3+} magnons.

Yb^{3+} single-ion CEF transition from the ground state to the first excited doublet (see the CEF calculations in Ref. [23]).

Figure 2 shows constant-energy slices in the $(H0L)$ plane taken around energies $E = 1, 20, 40, 60$ meV at $T = 2$ K (left) and $T = 15$ K (right). Slices at $E = 40, 60$ meV show the clean spin-wave excitations caused by the Fe-Fe interaction for both temperatures, and one can see the redistribution of the INS intensity, which is concentrated either along the L or H direction, at $T = 15$ and 2 K, respectively, as expected from the known SR transition of the Fe moments. For $E = 1$ and 20 meV, one can see additional intensity, which corresponds to the ground state splitting and first excited CEF doublet of Yb^{3+}, respectively. In contrast to the conventional CEF excitations without significant $\mathbf{Q}$ dependence, here one can see that the INS intensity has an X shape (hourglass) for both temperatures, which does not change through the SR transition for both excitations [35].

Due to the experimental resolution limitations ($\Delta E \approx$ 3 meV for our setup), we were not able to precisely extract the gap values from the SEQUOIA data sets and performed additional measurements with $E_i = 12$ meV on the CNCS instrument. Figure 3(d) shows the energy cuts taken along the (101) direction at $T = 2$ and 15 K. In order to extract the gap

value, we took the inflection points, as shown in Fig. 3(d), and found $\Delta = 4.03(5)$ meV for 2 K and $\Delta = 4.88(5)$ meV for 15 K.

B. Low-energy INS data

According to specific-heat measurements published previously [36], the Yb^{3+} ground-state doublet has a splitting of 1 meV, therefore, in order to investigate the spin dynamics of the Yb subsystem, we performed measurements on the CNCS instrument with $E_i = 3$ meV in the $(H0L)$ and $(0KL)$ scattering planes. The experimentally observed intensity maps, $I(\mathbf{Q}, E)$ along the $(00L)$ direction, are shown in Figs. 3(a) and 3(b) for temperatures below and above the SR transition. The excitation spectrum at $T = 2$ K is dominated by a high-intensity sharp mode, which disperses only along the Q_L direction. At the zone center, this mode peaks at $E_1 \approx 1$ meV. We also observe a weak dispersionless excitation at $E_2 \approx$ 1.5 meV and a continuum centered at $E_3 \sim 1.8$ meV with dispersive boundaries and a bandwidth of $\Delta E \approx 0.3$ meV at the zone center. Above T_{SR}, a different spectrum emerges. A bow-tie-shaped continuum arises at $E \approx 0.6$ meV with a sharp mode observed at the lower boundary. The low-intensity

excitation E_2 and the continuum E_3, present at $T = 2$ K, totally disappear. Figure 3(c) shows energy cuts taken at $\mathbf{Q} = (001)$. One can see that all E_1, E_2, and E_3 peaks, observed at $T = 2$ K, could be described with a single Gaussian function, whereas a cut, taken through the center of the continuum at $T = 10$ K, consists of two peaks: a relatively narrow, intense peak centered at $E = 0.47$ meV, and a second broad peak at $E = 0.63$ meV. All observed excitations have negligible dispersion along other directions (see additional figures in Ref. [23]), indicating that the Yb moments form weakly coupled spin chains running along the c axis despite the three-dimensional perovskite structure, in a similar fashion as it was proposed for isostructural YbAlO$_3$ [18].

Moreover, in both spectra taken above and below T_{SR}, we observed a second "shadow" mode [37] with similar dispersion, but shifted periodicity. It has no intensity at $Q_K = 0$, but becomes visible at higher Q_K. We describe the spectrum taken at 2 K using a LSWT calculation and show that this mode is associated with the buckling of the Yb chains along the b axis [38] (details are presented in Ref. [23]).

C. Effect of the polarization factor on the INS spectra

Before one can start a discussion or some quantitative analysis of the spin dynamics in magnetic materials, it is very important to establish the static magnetic structure, which, in the general case, could be obtained from neutron diffraction measurements. The magnetic structure of the Fe subsystem was determined and published for both $\Gamma4$ and $\Gamma2$ magnetic configurations [13,14,17,39]. To the best of our knowledge, there is no magnetic ordering of the Yb sublattice down to $T \approx 100$ mK [40]. Therefore we can only discuss the preferred orientation of Yb moments, which can be caused by both Yb single-ion anisotropy due to the CEF [41] and Yb-Fe interactions, including both dipole-dipole and exchange terms. Previous measurements of YbFeO$_3$ using Mössbauer spectroscopy [42], as well as theoretical work by Yamaguchi [43], concluded that the Yb moments are strongly coupled to the Fe subsystem and therefore, Yb spins rotate from the a to c axis at T_{SR}. Our qualitative analysis of the polarization of INS presented below disagrees with this conclusions.

The polarization factor of neutron scattering affects the final scattering intensity, because only magnetic moment components perpendicular to the scattering vector $\mathbf{Q}$ contribute to the magnetic cross section. The longitudinal component S^{zz} that is mostly contributed from the moments along the Q_i ($i = H, K, L$) direction should follow the polarization factor:

$$p_i = 1 - \frac{(Q_i)^2}{(Q_H)^2 + (Q_K)^2 + (Q_L)^2}. \tag{1}$$

Taking into account the form factor of the magnetic ion $|f(\mathbf{Q})|$, the integrated scattered intensity has the $\mathbf{Q}$ dependence

$$\int I(\mathbf{Q}, E)dE \propto |f(\mathbf{Q})|^2 \cdot p_i. \tag{2}$$

Equation (2) predicts a cone-shaped scattering, and the strongest intensity is recorded $\mathbf{Q} \perp \mathbf{Q}_i$.

The CEF lifts the degeneracy of the $4f^{13}$ electronic configuration of Yb^{3+} into four Kramers doublets. Since the spin dynamics at the energy scale of $E \approx 1$ meV is associated with
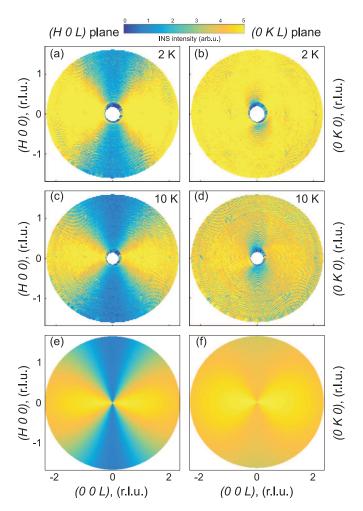

FIG. 4. Measured [(a)–(d)] and calculated [(e) and (f)] constant energy plots in the $(H0L)$ (left column) and $(0KL)$ (right column) scattering plane at [(a) and (b)] $T = 2$ and [(c) and (d)] 10 K. The scattering intensity was integrated within $E = [0.8, 1.2]$ and $[0.4, 0.8]$ meV for $T = 2$ and 10 K, respectively.

fluctuations of Yb moments, the low-energy INS should reflect the wavefunctions anisotropy of the Yb ground-state doublet. The CEF is controlled by the near neighbor coordination, which is little affected by isostructural substitution of rare-earth ions in the RFeO$_3$ family. Therefore, in order to estimate an effect of crystal field and the ground state wavefunctions of Yb^{3+}, we used CEF parameters determined for NdFeO$_3$ [44]. We found that the Yb moments have a strong Ising-like anisotropy and lie in the ab plane forming an angle within $\alpha = \pm21°$ to the a axis (See [23,45,46] for details). Figure 4 presents $\mathbf{Q}$-dependencies of INS scattering taken within $(H0L)$ and $(0KL)$ planes for temperatures above and below the SR transition [47]. At both temperatures, $T = 2$ and 10 K, the INS intensity integrated over the range of Yb-spin excitations has a strong anisotropy in the $(H0L)$ plane, whereas the signal in the $(0KL)$ plane is almost isotropic. In order to describe such scattering intensity, we calculated $\mathbf{Q}$ dependencies of the INS intensity in the both $(H0L)$ and $(0KL)$ planes, assuming that the Yb moments lie in the ab plane with $\alpha = \pm21°$ degree to the a axis. In this case, Eq. (1) describing a polarization

factor of the neutron scattering can be rewritten in a following forms:

$$p_{(H0L)} = \frac{(Q_L)^2 + \cos^2\alpha(Q_H)^2}{(Q_H)^2 + (Q_L)^2}, \qquad (3)$$

$$p_{(0KL)} = \frac{(Q_L)^2 + \sin^2\alpha(Q_K)^2}{(Q_K)^2 + (Q_L)^2}, \qquad (4)$$

for $(H0L)$ and $(0KL)$ scattering planes, respectively. Because we assumed, that the magnetic moments of the Yb lie close to the [100] direction, INS intensity, calculated for the $(H0L)$ plane, has a strong anisotropy [Fig. 4(e)]. On the other hand, the polarization factor of the INS scattering in the $(0KL)$ plane has only a weak **Q** dependence with maximums of the intensity along the $(00L)$ direction as shown in Fig. 4(f). At both temperatures, $T = 2$ and 10 K, the INS intensity integrated over the range of Yb spin excitations is qualitatively consistent with the calculations, as one can see in Figs. 4(a)–4(f). Thus, at both temperatures below and above SR transition, the fluctuations we observed are dominated by the longitudinal component S^{zz} along the easy axis of Yb magnetization.

Note that the INS intensity of the first CEF excitation at $E \approx 20$ meV is concentrated along the (100) direction [see Figs. 2(c) and 2(d)], perpendicular to the low-energy $E \approx 1$ meV excitation. A strong similarity of Yb excitations at $T = 2$ and 10 K confirms that the magnetic anisotropy and the symmetry of wave functions of Yb^{3+} remains the same despite the SR transition, contrary to previous reports [42,43]. This fact is also in a good agreement with the magnetization data as well as the results of the CEF calculations for YbFeO$_3$ [23], showing that the ground-state doublet of Yb has a strong Ising-like anisotropy with easy-axis lying close to the a axis, whereas the first excited doublet, which has a different symmetry, is located at the energy transfer of ~ 20 meV, and therefore, can not influence the low-temperature magnetic properties.

IV. ZERO-FIELD MEASUREMENTS: INTERPRETATION

A. Magnetic Hamiltonian of YbFeO₃

Coming to the quantitative description of the experimental results, we want to point out that in the general case Hamiltonian describing the spin dynamics of YbFeO$_3$ for both rare-earth and Fe sublattices should take into account three different terms:

$$\mathcal{H} = \mathcal{H}_{\text{Fe-Fe}} + \mathcal{H}_{\text{Yb-Yb}} + \mathcal{H}_{\text{Fe-Yb}}, \qquad (5)$$

where the first two terms describe exchange interactions and single-ion anisotropies within Fe and Yb subsystems, respectively. The third term is an effective interaction between the Fe and Yb subsystems, including both dipole-dipole and exchange terms. A few decades ago, Yamaguchi proposed and analyzed a model, which took into account all symmetric and antisymmetric exchange interactions within the Fe sublattice as well as interactions between Fe and R sublattices, whereas the interactions and anisotropy within the R sublattice were neglected [43]. The excitation spectrum of this model consists of a number of entangled collective Fe-R spin-wave modes, as was shown for many other compounds with magnetic interaction between different sublattices [48–53].

In contrast, for both temperatures, below and above the SR transition, in our experimental spectra, we were able to separate two groups of collective excitations with rather different energy scales: (i) quasi-1D mode, caused by Yb-Yb exchange along the c axis at $E \approx 1$ meV [see Figs. 3(a) and 3(b)] and (ii) gapped high-energy spin-waves modes [see Figs. 1(a) and 1(b)], similar to other orthorhombic orthoferrites and associated with Fe-Fe exchange and Fe single-ion anisotropy [19,20]. Therefore, in order to phenomenologically describe the main features of the observed spin dynamics, we decouple the Yb and Fe subsystems and construct the effective Heisenberg-like spin Hamiltonians for each of them separately.

Previously it was shown that in the RFeO$_3$, the influence of the Fe subsystem on the R moment can be described in terms of an effective field [54–56], and here we followed the approach of the "modified mean-field theory," recently developed for RFeO$_3$ [15,57,58]. Bazaliy *et al.* analyzed a free energy functional of ErFeO$_3$ [57]. They assumed that the ordered Fe subsystem polarizes nearly paramagnetic, strongly anisotropic moments of R-ions by an internal molecular field $\mathbf{H}^{\text{Fe}}$. In this model, one can take into account the influence of ordered Fe moments on the Yb subsystem with a simple Zeeman term and write down the magnetic Hamiltonian for the Yb moments in a form:

$$\mathcal{H}_{\text{Yb}} = \sum_{l,m,i} B_m^l O_m^l(\mathbf{J}_i^{\text{Yb}}) + J \sum_{\langle i,j \rangle} \mathbf{J}_i^{\text{Yb}} \cdot \mathbf{J}_j^{\text{Yb}} + \mathbf{H}^{\text{Fe}} \sum_i \mathbf{J}_i^{\text{Yb}}, \quad (6)$$

where the first term is an one-site CEF Hamiltonian in Stevens notations [59,60], the second term is the Yb-Yb intersite Heisenberg exchange interaction, and the third term represents an influence of the Fe molecular field on the Yb magnetic subsystem.

Now, let us focus on the choice of the model Hamiltonian for description of the magnetic structure and spin dynamics of the Fe subsystem. Without taking into account the Yb subsystem, it could be written in the following form:

$$\mathcal{H}_{\text{Fe}} = \sum_{\langle i,j \rangle} \mathbf{S}_i^{\text{Fe}} \cdot J_{ij} \cdot \mathbf{S}_j^{\text{Fe}} - \sum_i \mathbf{S}_i^{\text{Fe}} \cdot K_i \cdot \mathbf{S}_i^{\text{Fe}}, \qquad (7)$$

where J_{ij} is a 3×3 matrix, containing both symmetric and Dzyaloshinskii-Moriya (DM) Fe-Fe intersite exchange interactions and K_i is a diagonal 3×3 matrix describing the effective single-ion anisotropy of the Fe moments. Due to the orthorhombic symmetry of the Fe environment, the anisotropy matrix K_i contains two nonequivalent constants K_a and K_c. In this Hamiltonian, the first term dictates an overall shape and maximum energy of the Fe excitations, the anisotropy determines a magnetic ground state [61] and gives rise to the gap in the Fe magnon spectrum [19]. In RFeO$_3$ with nonmagnetic R-ions, a dominating K_a stabilizes the $\Gamma 4$ phase, whereas in compounds with magnetic R, the R-Fe interaction induces renormalization of the effective anisotropy constants. At $T \approx T_{\text{SR}}$, K_a and K_c become approximately equal, and the term $\propto (S^z)^4$ controls the rotation of the Fe spins [61]. Below the SR transition $K_c > K_a$ stabilizes the $\Gamma 2$ phase. Having in mind that (i) the high-energy magnons in YbFeO$_3$ do not change through the SR transition and (ii) there are no collective Fe-Yb modes, we describe the evolution of the magnetic ground state and high-energy spin dynamics of the Fe subsystem, introducing a temperature dependency
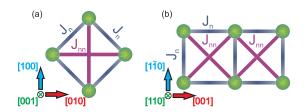
of the effective anisotropy constants $K_a'(T)$ and $K_c'(T)$ due to the Yb-Fe interaction. Note that the K_c' dominates in $\Gamma2$, while K_a' dominates in the $\Gamma4$ phase [62]. In Ref. [23], we present a detailed analysis of the free energy functional of YbFeO$_3$ at temperatures close to T_{SR} and clarify, why the R-Fe exchange interaction leads to the SR transition and induces renormalization of the effective anisotropy constants.

We should point out that this is an entirely phenomenological approach, which, however, describes the details of the magnetic behavior of YbFeO$_3$ as well as most of the features of the observed spin dynamics. Construction of the microscopically full magnetic Hamiltonian without decoupling of the Fe and Yb subsystems goes far beyond the scope of our work, but we hope that the results of our study will motivate further theoretical work on the unconventional spin dynamics in YbFeO$_3$ and explain the microscopic mechanism of the R-Fe interaction in rare-earth orthoferrites.

B. Linear spin-wave model for the Fe magnons

As the first step, we focus on high-energy spin dynamics of the Fe subsystem. Recently, a general Hamiltonian [Eq. (7)], describing the magnetic properties of the Fe subsystem, was written in a following form, in order to describe spin structure and dynamic properties of the isostructural YFeO$_3$ [19]:

$$
\mathcal{H}_{\text{Fe}} = J_{nn} \sum_{\langle i,j \rangle} \mathbf{S}_i \mathbf{S}_j + J_{nnn} \sum_{\langle i,j \rangle'} \mathbf{S}_i \mathbf{S}_j - D_1 \sum_{\substack{R_j = R_i \\ +a(x \pm y)}} \mathbf{S}_i \times \mathbf{S}_j
$$

$$
- D_2 \sum_{\substack{R_j = R_i \\ +a(x \pm y)}} \mathbf{S}_i \times \mathbf{S}_j - K_a' \sum_i \left(S_i^x\right)^2 - K_c' \sum_i \left(S_i^z\right)^2.
$$

$$(8)$$

It contains two isotropic exchange interactions between nearest-neighbor and next-nearest-neighbor Fe ions (see Fig. 5), two DM exchange interactions within the ab plane, and two effective easy-axis anisotropy constants K_a' and K_c'. As we discussed above, in order to take into account Yb-Fe exchange interaction and stabilize the correct ground state, either $\Gamma4$ or $\Gamma2$, we assume that the effective K_a' and K_c' are changing with temperature. A large gap in the magnon spectra $\Delta \approx 4$ meV [see Fig. 3(d)], observed at both temperatures, $T > T_{SR}$ and $T < T_{SR}$, indicates an easy-axis character of the dominating anisotropy constant.

In rare-earth orthoferrites, DM exchange interactions give rise to the canted magnetic structure and an optical magnon branch at $E \approx 65$ meV [19]. However, the effective values of the DM parameters are rather small and, therefore, the

corresponding branches have a vanishingly small spectral intensity, so we could not observe them in our INS data. On the other hand, knowing the canting angles $\theta = 0.35°$ and $\phi = 0.18°$ [63] from the room-temperature neutron diffraction measurements [17], we calculated both D_1 and D_2 using Eq. (3,4) from [19].

We would like to note that the first two symmetric Heisenberg exchange interactions define the energy scale and overall shape of the magnon branches. The dominating anisotropy constant determines the ground state ($\Gamma4$ or $\Gamma2$) and gives rise to the gap in the excitation spectrum. The presence of the DM exchange leads to a spin canting of the Fe spins [17,19]. The DM terms and the second anisotropy constant play a minor role in the spectrum and their spectroscopic determination requires additional careful measurements [20]. Therefore, to reproduce the magnon excitations of the Fe subsystem, we used Hamiltonian (8), with J_{nn}, J_{nnn}, K_a' (for $T > T_{SR}$), and K_c' (for $T > T_{SR}$) as free parameters, whereas D_1 and D_2 constants were calculated from the canting angles and fixed for both temperatures. In order to derive parameters from the experimental spectra, we fit the experimental data at 28 different points of $\mathbf{Q}$ space along nonequivalent directions and extracted the energy and intensities of the magnon mode. Then, we fitted these points to our model Hamiltonian using SPINW software [30]. The best sets of exchange parameters for both phases are shown in Table I. Calculated dispersion curves, shown in Figs. 1(a) and 1(b) as the white dashed lines, are in good agreement with experimental data.

C. Quantum quasi-1D excitations in the Yb subsystem

Having described the high-energy magnetic excitations of the Fe sublattice, we now discuss the low-energy magnetic excitations of the Yb^{3+} moments observed in YbFeO$_3$. The CEF term in Hamiltonian (6) gives a large splitting of the $J = 7/2$ multiplet of Yb^{3+}. The energy gap between the ground state and the first excited doublet is $\Delta = 20$ meV [64]. Therefore, for the description of the low-energy spin dynamics, we can take into account the ground-state doublet alone and use the pseudospin $S = 1/2$ approximation. As we mentioned above, nearest-neighbor Yb moments are coupled along the c axis by an exchange interaction. In a simple approximation, the influence of the Fe subsystem on the Yb ions could be taken into account via the effective molecular field, which is created by the Fe sublattice as was discussed previously. We transform Eq. (6) into the one-dimensional XXZ $S = 1/2$ Hamiltonian:

$$
\mathcal{H}_{\text{Yb}} = J_z \sum_i S_i^z S_{i+1}^z + J_{xy} \sum_i \left(S_i^x S_{i+1}^x + S_i^y S_{i+1}^y\right)
$$

$$
+ \sum_i \mathbf{H}_{\text{ef}} \cdot \mathbf{S}_i,
$$

$$(9)$$

TABLE I. Parameters of the magnetic Hamiltonian (8) derived in this work. All values are given in meV.

Magnetic phase	J_{nn}	J_{nnn}	D_1	D_2	K_a'	K_c'
$\Gamma2$ ($T = 2$ K)	4.675	0.158	0.086	0.027	0	0.023
$\Gamma4$ ($T = 15$ K)	4.675	0.158	0.086	0.027	0.033	0

where the first two terms correspond to the anisotropic exchange interaction between the nearest-neighbor Yb along c axis, and the last term is an effective Zeeman term—sum of the external field and the molecular field of the Fe subsystem.

At temperatures $T < T_{SR}$, the net moment of the Fe subsystem is directed along the a axis, as shown in Fig. 1(c), creating a *longitudinal* field for Yb^{3+} spins. In order to describe the low-T spectrum, we performed calculations of the eigenstates of Eq. (9) using the zero temperature exact diagonalization of a finite chain ($L = 20$) with ALPS software [32,33]. A cosine-shape dispersion of the lowest excitation with a maximum at the zone center suggests that the exchange interaction is antiferromagnetic [23] and that the effective field $\mathbf{H}_{ef}$ is large in comparison to J_z and J_{xy}. In this case, all spins are parallel, $\langle S_n^z \rangle = S$ [6]. The excitation spectrum of such a fully polarized state is similar to that of a FM chain and was discussed in detail a few decades ago [65–70]. A single sharp mode with energy $E \approx 1$ meV occurs due to scattering by a single-flip quasiparticle. Besides, modes of an anisotropic FM or field-polarized AFM chain contain a two-kink bound state and a continuum consisting of pairs of independently propagating kinks. We found the cross section of two-kink states to be about two orders of magnitude weaker than that for the single-flip excitation, in agreement with the theoretical prediction [65]. In case of both $J_z > 0$ and $J_{xy} > 0$, the calculated two-magnon bound state mode lies above the continuum, which contradicts our experimental data [Fig. 3(a)]. Our data would be reproduced well for $J_z < 0$ and $J_{xy} > 0$. However, the situation when a single exchange bond has both FM and AFM correlations between different spin components seems to be unrealistic. Furthermore, the magnetic ground state of the isostructural $YbAlO_3$ was found to be AFM [18]. This question requires a separate theoretical study.

At temperatures $T > T_{SR}$, the Fe net moment reorients along the c axis, inducing a *transverse* field for the Yb spins [see Fig. 1(e)]. However, at $T = 10$ K, the observed superposition of a bow-tie-shaped spinonlike continuum with a sharp excitation at the bottom [see Fig. 3(b)], suggests that the Yb sublattice is in a partially polarized state, as if a weak longitudinal field were still present. A weak coupling between the magnetic chains in the ab plane, evident from a weak dispersion along H and K directions (see Figs. 5 and 6 in Ref. [23]), could be a possible explanation of the observed spectrum. Such coupling in a first approximation can be replaced by an effective longitudinal mean field [71,72]. The spin-excitation spectrum in a skew (H_x, H_z) field is indeed characterized by a combination of a continuum due to scattering by pairs of kinks, which interpolate between regions with magnetization "up" and "down" and a sharp mode created by single spin-flip quasiparticles. The finite temperature model of an XXZ chain is required to describe the details of the experimental spectra in this case.

V. MAGNETIC FIELD EFFECT ON THE LOW-ENERGY SPIN DYNAMICS

In previous sections, we assumed that the influence of the ordered Fe subsystem on the Yb subsystem can be taken into account via the effective molecular field, which rotates from the c to a-axis at T_{SR}. In this section, we present the results of INS measurements with magnetic field applied along all a, b, and c axes of the orthorhombic $YbFeO_3$ and show that the effect of the external magnetic field on the spin dynamics is similar to that of the internal Fe-induced field. The results of the measurements for the $\mathbf{H} \parallel [100]$ and $\mathbf{H} \parallel [010]$ are summarized in Fig. 6 [73].

First of all, let us consider the low-temperature ($T < T_{SR}$) spectra under the magnetic field along the a axis, Figs. 6(a)–6(c). In this case, Yb spins are already polarized along the easy a axis even without an external magnetic field. The external field leads to further Zeeman splitting of the ground state, whereas the total INS intensity of the excitation is decreasing.

At $T = 10$ K, $YbFeO_3$ is in the $\Gamma 2$ phase, and the net moment is directed along the c axis. Application of the magnetic field $\mathbf{H} \parallel [100]$ at this temperature has a dual effect: (i) it polarizes the Yb subsystem and (ii) induces a SR transition of Fe-moments $\Gamma 4 \rightarrow \Gamma 2$. According to the specific-heat measurements [23], at $T = 10$ K, such a SR transition takes place at $H \approx 4.3$ T. In our INS data [see Figs. 6(d)–6(f)], we observe Zeeman splitting, whereas the continuum, dominating at zero field, is rapidly suppressed and becomes undetectable already at $H = 3$ T. At $H = 5$ T, above the field-induced SR transition, the magnetic phase $\Gamma 2$ is stabilized. The spectra at both temperatures, $T = 2$ and 10 K, become identical. Assuming the linear dependence of the energy splitting within the low-temperature $\Gamma 2$ phase, we calculated an effective g factor $g_a^{\Gamma 2} = 4.135$.

In contrast to the relatively simple case of $\mathbf{H} \parallel [100]$, a magnetic field applied along the b axis qualitatively changes the excitation spectra. At temperatures below T_{SR} [Figs. 6(g) and 6(h)], the single-particle mode splits into two parallel modes, whereas above T_{SR} magnetic field up to 2 T has a minor effect on the spectra [see Figs. 6(i) and 6(j)] [74]. According to the our model, below T_{SR} the Yb moments have an Ising-like anisotropy, lie in the ab plane with $\alpha \approx \pm 21°$ to the a axis and are fully polarized by the molecular field of the Fe subsystem. Schematically, molecular-field-induced magnetic structure of the Yb subsystem below T_{SR} is shown in Fig. 6(k). Application of a magnetic field along the b axis lifts the degeneracy between neighbor magnetic chains, increasing the energy of fluctuations with the positive Yb moment projection on the b axis, $\alpha = +21°$, and decreasing the energy for the opposite direction, $\alpha = -21°$. A further increase in field would suppress the energy of the lower mode down to zero with a simultaneous polarization of Yb moments along the b axis.

In $YbFeO_3$, Yb moments are coupled in chains running along the c axis, creating the dispersion along the $(00L)$ direction. To apply a magnetic field along the c axis, an experimental arrangement with *horizontal* field is preferred, since only magnetic moment components perpendicular to the scattering vector $\mathbf{Q}$ contribute to the magnetic cross section, as we discussed in Sec. III C. Therefore, for INS measurements in this geometry, we oriented the sample in the $(H0L)$ scattering plane and used the triple-axis FLEXX instrument with the horizontal cryomagnet HM-1. However, due to the instrument restrictions (dark angles of the magnet) we were limited with the $\mathbf{Q}$ range from (0 0 0.5) to (0 0 1.1) for $k_f = 1.3$ Å^{-1}.

The magnetic-field–temperature phase diagram of $YbFeO_3$ reconstructed from the magnetic measurements is shown in
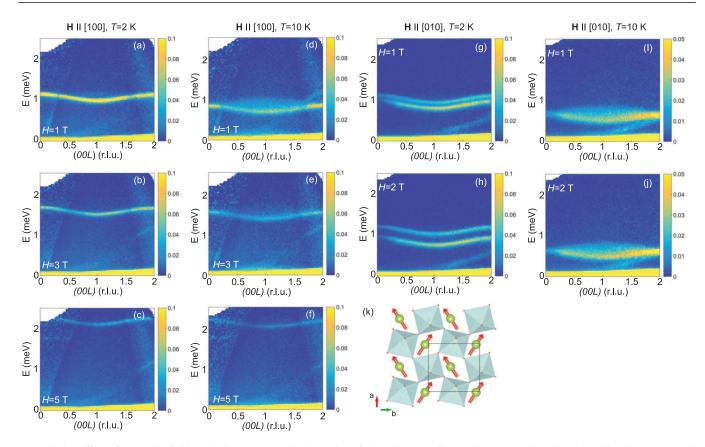
FIG. 6. Effect of magnetic field on the low-energy spin dynamics of YbFeO$_3$. Experimental spectrum along the (00L) direction, measured at magnetic fields along the [(a)–(c)] a and [(g)–(j)] b axes, at temperatures [(a)–(c),(g), and (h)] 2 and [(d)–(f),(i),and (j)] 10 K. A visible linear diagonal line on the spectra is due to an instrumental effect. (k) Sketch of the field-induced magnetic structure of Yb moments below T_{SR}.

Fig. 7(a). One can see that the low-T phase Γ2, where the weak net moment of the Fe subsystem is aligned along the a axis, could be suppressed by the magnetic field along the c axis. The critical field $H_{\text{crit}}^{\Gamma2\to\Gamma4}$ gradually increases with the temperature decreasing.

Inelastic spectra taken at $\mathbf{Q} = (001)$ and $H = 4$ T are described by the combination of two modes, a resolution-limited intense peak ("main" mode) and an additional broad peak at higher energy, see Fig. 7(b). We use two Gaussian functions for fitting the spectral line-shape. The low-temperature scans ($T = 2$ and 3 K) in the Γ2 phase show the largest contribution of the "main" mode. The center of the second peak is located very close to the first one. At $T = 4$ K, a field-induced SR transition occurs. The second peak shifts to higher energies and its intensity grows, whereas further increase in temperature has no major effect on the spectra.

Figure 7(c) shows magnetic field dependence of the "main" mode taken at different temperatures. The spectra taken at $T = 2$ and 4 K show that the excitation energy is always growing up in the Γ2 phase. However, we found different behavior of the "main" magnetic peak at $T = 6$, 8, and 10 K. First, the excitation energy goes down until the critical field $H_c^{\Gamma2\to\Gamma4}$ [see Fig. 7(a)], and it starts growing at higher fields. Thus, in the Γ2 phase, increasing field reduces the energy of the excitation, whereas in the Γ4 phase excitation energy rises with the field. We also calculated the effective g factor for the Γ4 phase, which was found to be $g_c^{\Gamma4} = 1.09$, almost four times smaller compared to a $g_a^{\Gamma2} = 4.135$.

VI. DISCUSSION AND CONCLUSIONS

A large number of independent parameters of the full microscopic spin Hamiltonian of YbFeO$_3$ [43] makes the analysis ambiguous and complicated. However, quantitatively, one can consider three energy scales $J_{\text{Fe-Fe}} \gg J_{\text{Fe-Yb}} > J_{\text{Yb-Yb}}$. Strong $J_{\text{Fe-Fe}}$ interaction induces an AFM ordering in the Fe subsystem with $T_N \approx 600$ K and its manifestations are clearly seen in high-temperature magnetic susceptibility or specific-heat measurements, magnetic neutron diffraction and INS spectra. The intermediate strength Yb-Fe interaction induces a spontaneous SR transition Γ4 → Γ2 at decreasing temperature, and can be extracted from the low-temperature magnetization and specific-heat measurements, but the presence of $J_{\text{Yb-Fe}}$ exchange does not introduce new collective Yb-Fe modes or hybridization. Finally, the weakest 1D Yb-Yb correlations create unusual low-energy excitation spectra, which include a two magnon bound state, "shadow" mode, a spinon continuum, etc. Note that on one hand, details of the Yb-Yb correlations are hidden for the most of the experimental macroscopic probes by dominating $J_{\text{Fe-Fe}}$ and $J_{\text{Fe-Yb}}$ interactions. On the other hand, an *ab initio* DFT calculation, which can be used to identify the 1D character of Yb correlations does also fail to capture weak Yb-Yb correlations, due to the low one-site symmetry of both magnetic ions and presence of a second magnetic subsystem with much larger exchange energy. Therefore high-resolution cold-neutron spectroscopy is a unique probe, which can explore details of the spin dynamics in the Yb subsystem and it is
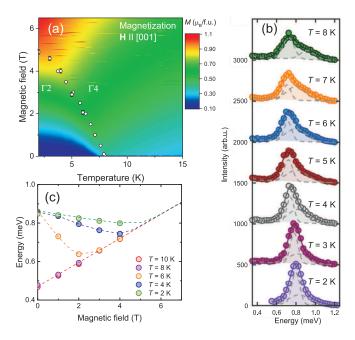
FIG. 7. Effect of magnetic field along the *c* axis on the low energy spin dynamics of YbFeO$_3$. (a) Magnetic-field–temperature phase diagram of YbFeO$_3$ taken at **H** applied along the *c* axis. Color-plot shows magnetization data. (b) Energy scans, measured on the FLEXX instrument at $H = 4$ T and $Q = (001)$ at various temperatures. Solid line is an overall fit of the magnetic signal. Dotted lines represent two Gaussian functions, used for the fitting. (c) Magnetic field dependence of the "main mode" peak as a function of magnetic field. Dotted lines are drawn to guide the eyes.

not surprising, that despite more than 60 years of investigations of rare-earth orthoferrites [14], quasi-one-dimensional Yb-Yb correlations have never been observed.

The main aim of this work is to present an experimental observation of the decoupled spin dynamics of the Fe and Yb subsystems, coexisting on different energy scales and to give a phenomenological description of the observed spectra. We constructed spin Hamiltonians for each magnetic subsystem separately. The key simplification was to treat Yb-Fe interaction in terms of an effective "mean-field" approximation, instead of constructing a combined microscopic Hamiltonian, which should include both magnetic subsystems, and, therefore, terms $\propto S^{Fe} \cdot S^{Yb}$.

We show that the magnetic structure and spin dynamics of the Fe subsystem can be well described using the semiclassical LSWT. This model takes into account the nearest neighbor exchange interaction and assumes the dominating effective easy-axis anisotropy constants K'_a or K'_c for the $\Gamma 4$ or $\Gamma 2$ phases, respectively.

Because the low-energy excitations were found to have a dispersion along the *c* axis only, we concluded that the Yb nearest-neighbor AFM exchange interaction along the *c* axis dominates the exchange interactions within the *ab* plane, despite the 3D crystal structure of YbFeO$_3$. For the description of the Yb dynamics, we propose a 1D-XXZ $S = 1/2$ [Eq. (9)] Hamiltonian with the additional Zeeman term describing the effective interaction with the Fe subsystem. The calculated excitation spectrum is in a reasonable agreement with the low-temperature experimental spectrum, when the molecular

field of the Fe subsystem is longitudinal to the easy axis of the Yb moments (at $T < T_{SR}$). The observed spectrum consists of the sharp intense single-magnon mode and two multi-magnon excitations: the dispersionless two-magnon bound state and the two-magnon continuum. At $T > T_{SR}$ in the $\Gamma 4$ phase, the molecular field of the Fe subsystem is aligned along the *c* axis and transverse to the easy axis of Yb moments, which lies in the *ab* plane, with $\alpha = 21°$ to the *a* axis [23]. We found that the single particle mode is shifted down in energy and accompanied by a broad spinon continuum, as it was reported for many other $S = 1/2$ 1D magnets [5,6,75,76].

We performed calculations of the eigenstate spectrum for the 1D XXZ model including the transverse field (9) but could not find any set of parameters, which satisfactorily describes the experimentally observed excitations [23]. The apparent reason for such disagreement is that the model Hamiltonian (9) is oversimplified and not sufficient to describe the details of the low-energy spin dynamics in YbFeO$_3$ at finite temperatures. We assume three main approximations: (i) we took into account the Yb-Yb exchange interaction along the *c* axis only; (ii) the $J = 7/2$ multiplet of Yb^{3+} was substituted by the two-level pseudo-$S = 1/2$ system; (iii) we considered Yb-Fe exchange interaction as an effective internal field, following Refs. [15,57,58]. The two first approximations are based on a number of experimental facts: 1D dispersion of Yb excitations; broad maximum on the temperature dependent magnetic susceptibility of the YbAlO$_3$, associated with the 1D spin correlations [18]; spinonlike excitations above T_{SR}; the large CEF gap in the INS spectrum $\Delta = 20$ meV. The third approximation is a common simplification, used for systems with several magnetic sublattices, where one energy scale significantly exceed others [77–79].

Besides, instead of the temperature dependent dynamical spin susceptibility $\chi''(Q, \hbar\omega)$ measured at the INS experiment, we calculated the zero-temperature eigenstates of the spin Hamiltonian. In the low-temperature case $T < T_{SR}$, we have an energy hierarchy of $H^{Fe} \gg J^{Yb-Yb} \gg T$, and the calculated spectrum is split into the series of well define modes as clearly seen in Fig. 7 in Ref. [23]. Above the T_{SR}, $H^{Fe} \sim T > J$, and zero-T calculations become inapplicable. Finite temperature effects should be taken into account in order to describe the dynamical spin susceptibility.

In summary, we present a comprehensive INS study of the spin dynamics in YbFeO$_3$ at temperatures close to the SR transition and in magnetic fields applied along three crystallographic directions. We constructed an effective model describing spin dynamics and static magnetic structure of Fe moments for both temperatures above and below T_{SR} assuming the temperature dependence of the effective single-ion anisotropy constants K'_a and K'_c. In the low-energy magnetic spectra we observed an unusual transition between two regimes of the quasi-1D Yb fluctuations, induced by the rotation of the Fe molecular field, which serves as an intrinsic "tuning parameter." Our model Hamiltonian describes the main features of the low-temperature spectrum, whereas for the correct description of the spectrum at $T > T_{SR}$ further theoretical work will have to be done. We leave several open questions here: (1) what is the origin of the quasi-1D behavior within the Yb subsystem? (2) How to describe the unusual Yb excitation spectrum at $T > T_{SR}$ with coexisting spinon

and magnon modes? (3) What is the correct microscopical approach to describe the Fe-Yb exchange interaction instead of the mean-field approximation? We hope that the presented INS data and intriguing underlying physical phenomena would motivate further theoretical studies on $YbFeO_3$ and renew the interest to the rich physics of rare-earth orthoferrites in general, along with other materials with a coexistence of several magnetic subsystems on different energy scales.

[1] S. Sachdev, *Quantum Phase Transitions* (Cambridge University Press, New York, 2011).

[2] O. Stockert and F. Steglich, Unconventional quantum criticality in heavy-fermion compounds, Annu. Rev. Condens. Matter Phys. **2**, 79 (2011).

[3] Q. Si and F. Steglich, Heavy fermions and quantum phase transitions, Science **329**, 1161 (2010).

[4] F. D. M. Haldane, 'Spinon Gas' Description of the $S = \frac{1}{2}$ Heisenberg Chain with Inverse-Square Exchange: Exact Spectrum and Thermodynamics, Phys. Rev. Lett. **66**, 1529 (1991).

[5] D. A. Tennant, T. G. Perring, R. A. Cowley, and S. E. Nagler, Unbound Spinons in the $S = \frac{1}{2}$ Antiferromagnetic Chain $KCuF_3$, Phys. Rev. Lett. **70**, 4003 (1993).

[6] M. Mourigal, M. Enderle, A. Klöpperpieper, J.-S. Caux, A. Stunault, and H. M. Rønnow, Fractional spinon excitations in the quantum Heisenberg antiferromagnetic chain, Nat. Phys. **9**, 435 (2013).

[7] S-W. Cheong and M. Mostovoi, Multiferroics: a magnetic twist for ferroelectricity, Nat. Mater. **6**, 13 (2007).

[8] D. Khomskii, Classifying multiferroics: Mechanisms and effects, Physics **2**, 20 (2009).

[9] Y.-J. Ke, X.-Q. Zhang, Y. Ma, and Z.-H. Cheng, Anisotropic magnetic entropy change in $RFeO_3$ single crystals (R = Tb, Tm, or Y), Sci. Rep. **6**, 19775 (2016).

[10] A. V. Kimel, A. Kirilyuk, P. A. Usachev, R. V. Pisarev, A. M. Balbashov, and Th. Rasing, Ultrafast non-thermal control of magnetization by instantaneous photomagnetic pulses, Nature (London) **435**, 655 (2005).

[11] J. A. de Jong, A. V. Kimel, R. V. Pisarev, A. Kirilyuk, and Th. Rasing, Laser-induced ultrafast spin dynamics in $ErFeO_3$, Phys. Rev. B **84**, 104421 (2011).

[12] J. Jiang, Z. Jin, G. Song, X. Lin, G. Ma, and S. Cao, Dynamical spin reorientation transition in $NdFeO_3$ single crystal observed with polarized terahertz time domain spectroscopy, Appl. Phys. Lett. **103**, 062403 (2013).

[13] R. L. White, Work on the magnetic and spectroscopic properties of the rare-earth orthoferrites, J. Appl. Phys. **40**, 1061 (1969).

[14] R. M. Bozorth, V. Kramer, and J. P. Remeika, Magnetization in Single Crystals of Some Rare-Earth Orthoferrites, Phys. Rev. Lett. **1**, 3 (1958).

[15] Ya. B. Bazaliy, L. T. Tsymbal, G. N. Kakazei, V. I. Kamenev, and P. E. Wigen, Measurements of spin reorientation in $YbFeO_3$ and comparison with modified mean-field theory, Phys. Rev. B **72**, 174403 (2005).

[16] V. P. Plakhtij, Yu. P. Chernenkov, M. N. Bedrizova, and Zh. Shvejtser, Experimental proof of the existence of a weak antiferromagnetic component in yttrium orthoferrite, J. Exp. Theor. Phys. **80**, 2465 (1981).

[17] V. P. Plakhty, Yu. P. Chernenkov, and M. N. Bedrizova, Neutron diffraction study of weak antiferromagnetism in ytterbium orthoferrite, Solid State Commun. **47**, 309 (1983).

[18] P. Radhakrishna, J. Hammann, M. Ocio, P. Pari, and Y. Allain, Antiferromagnetic ordering in the ytterbium aluminum perovskite $YbAlO_3$, Solid State Commun. **37**, 813 (1981).

[19] S. E. Hahn, A. A. Podlesnyak, G. Ehlers, G. E. Granroth, R. S. Fishman, A. I. Kolesnikov, E. Pomjakushina, and K. Conder, Inelastic neutron scattering studies of $YFeO_3$, Phys. Rev. B **89**, 014420 (2014).

[20] K. Park, H. Sim, J. C. Leiner, Y. Yoshida, J. Jeong, S.-i Yano, J. Gardner, P. Bourges, M. Klicpera, V. Sechovský, M. Boehm, and J.-G. Park, Low-energy spin dynamics of orthoferrites $AFeO_3$ (A = Y, La, Bi), J. Phys.: Condens. Matter. **30**, 235802 (2018).

[21] S. M. Shapiro, J. D. Axe, and J. P. Remeika, Neutron-scattering studies of spin waves in rare-earth orthoferrites, Phys. Rev. B **10**, 2014 (1974).

[22] A. Gukasov, U. Steigenberger, S. N. Barilo, and S. A. Guretskii, Neutron scattering study of spin waves in $TbFeO_3$, Physica B **234–236**, 760 (1997).

[23] See Supplemental Material at http://link.aps.org/supplemental/10.1103/PhysRevB.98.064424 for details of calculations, magnetization and specific heat measurements.

[24] L. N. Bezmaternykh, V. G. Mashchenko, N. A. Sokolova, and V. L. Temerov, Growth of iron garnet single crystals on a rotating carrier from $BaOB_2O_3$ fluxes, J. Cryst. Growth **69**, 407 (1984).

[25] G. Ehlers, A. Podlesnyak, J. L. Niedziela, E. B. Iverson, and P. E. Sokol, The new cold neutron chopper spectrometer at the spallation neutron source: design and performance, Rev. Sci. Instrum. **82**, 085108 (2011).

[26] G. Ehlers, A. Podlesnyak, and A. I. Kolesnikov, The cold neutron chopper spectrometer at the Spallation Neutron Source - A review of the first 8 years of operation, Rev. Sci. Instrum. **87**, 093902 (2016).

[27] G. E. Granroth, A. I. Kolesnikov, T. E. Sherline, J. P. Clancy, K. A. Ross, J. P. C. Ruff, B. D. Gaulin, and S. E. Nagler, SEQUOIA: A newly operating chopper spectrometer at the SNS, J. Phys.: Conf. Ser. **251**, 012058 (2010).

[28] O. Arnold, J. C. Bilheux, J. M. Borreguero, A. Buts, S. I. Campbell, L. Chapon, M. Doucet, N. Draper, R. Ferraz Leal,

M. A. Gigg, V. E. Lynch, A. Markvardsen, D. J. Mikkelson, R. L. Mikkelson, R. Miller, K. Palmen, P. Parker, G. Passos, T. G. Perring, P. F. Peterson, S. Ren, M. A. Reuter, A. T. Savici, J. W. Taylor, R. J. Taylor, R. Tolchenov, W. Zhou, and J. Zikovsky, Mantid – Data analysis and visualization package for neutron scattering and μSR experiments, Nucl. Instrum. Methods Phys. Res. Sect. A **764**, 156 (2014).

[29] R. A. Ewings, A. Buts, M. D. Le, J. van Duijn, I. Bustinduy, and T. G. Perring, HORACE: Software for the analysis of data from single crystal spectroscopy experiments at time-of-flight neutron instruments, Nucl. Instrum. Methods Phys. Res. Sect. A **834**, 132 (2016).

[30] S. Toth and B. Lake, Linear spin wave theory for single-Q incommensurate magnetic structures, J. Phys.: Condens. Matter **27**, 166002 (2015).

[31] http://www.mcphase.de; M. Rotter, Using McPhase to calculate magnetic phase diagrams of rare earth compounds, J. Magn. Magn. Mater. **272-276**, E481 (2004).

[32] B. Bauer, L.D. Carr, H. G. Evertz, A. Feiguin, J. Freire, S. Fuchs, L. Gamper, J. Gukelberger, E. Gull, S. Guertler, A. Hehn, R. Igarashi, S. V. Isakov, D Koop, P. N. Ma, P. Mates, H. Matsuo, O. Parcollet, G Pawłowski, J. D. Picon, L. Pollet, E. Santos, V. W. Scarola, U. Schollwöck, C. Silva, B. Surer, S. Todo, S Trebst, M. Troyer, M. L. Wall, P. Werner, and S. Wessel, The ALPS project release 2.0: Open source software for strongly correlated systems, J. Stat. Mech. Theory Exp. (2011) P05001.

[33] A. F. Albuquerque, F. Alet, P. Corboz, P. Dayal, A. Feiguin, S. Fuchs, L. Gamper, E. Gull, S. Gürtler, A. Honecker, R. Igarashi, M. Körner, A. Kozhevnikov, A. Läuchli, S. R. Manmana, M. Matsumoto, I. P. McCulloch, F. Michel, R. M. Noack, G Pawłowski, L. Pollet, T. Pruschke, U. Schollwöck, S. Todo, S. Trebst, M. Troyer, P. Werner, and S. Wessel, The ALPS project release 1.3: Open-source software for strongly correlated systems, J. Magn. Magn. Mater. **310**, 1187 (2007).

[34] M. D. Le, D. L. Quintero-Castro, R. Toft-Petersen, F. Groitl, M. Skoulatos, K.C. Rule, and K. Habicht, Gains from the upgrade of the cold neutron triple-axis spectrometer FLEXX at the BER-II reactor, Nucl. Instrum. Methods Phys. Res. Sect. A **729**, 220 (2013).

[35] The INS intensities, integrated in the energy range $E =$ [0.5, 1.5] meV, are rather noisy due to the proximity of the elastic line, and the details of the **Q** distribution of the low-energy magnetic signal could be extracted from the CNCS data much more clear, as shown in Fig. 4.

[36] M. R. Moldover, G. Sjolander, and W. Weyhmann, Second-Order Nature of the Spin-Reorientation Phase Transitions in YbFeO₃, Phys. Rev. Lett. **26**, 1257 (1971).

[37] I. Cabrera, J. D. Thompson, R. Coldea, D. Prabhakaran, R. I. Bewley, T. Guidi, J. A. Rodriguez-Rivera, and C. Stock, Excitations in the quantum paramagnetic phase of the quasi-one-dimensional Ising magnet CoNb₂O₆ in a transverse field: Geometric frustration and quantum renormalization effects, Phys. Rev. B **90**, 014418 (2014).

[38] M. Marezio, J. P. Remeika, and P. D. Dernier, The crystal chemistry of the rare earth orthoferrites, Acta Crystallogr. B **26**, 2008 (1970).

[39] W. C. Koehler, E. O. Wollan, and M. K. Wilkinson, Neutron diffraction study of the magnetic properties of rare-earth-iron perovskites, Phys. Rev. **118**, 58 (1960).

[40] We carried out neutron diffraction measurements and found no extra magnetic peaks or intensity changing down to $T \approx$ 100 mK.

[41] L. S. Wu, S. E. Nikitin, M. Frontzek, A. I. Kolesnikov, G. Ehlers, M. D. Lumsden, K. A. Shaykhutdinov, E-J. Guo, A. T. Savici, Z. Gai, A. S. Sefat, and A. Podlesnyak, Magnetic ground state of the Ising-like antiferromagnet DyScO₃, Phys. Rev. B **96**, 144407 (2017).

[42] G. R. Davidson, B. D. Dunlap, M. Eibschütz, and L. G. van Uitert, Mössbauer study of Yb spin reorientation and low-temperature magnetic configuration in YbFeO₃, Phys. Rev. B **12**, 1681 (1975).

[43] T. Yamaguchi, Theory of spin reorientation in rare-earth orthochromites and orthoferrites, J. Phys. Chem. Solids **35**, 479 (1974).

[44] R. Przenioslo, I. Sosnowska, M. Loewenhaupt, and A. Taylor, Crystal field excitations of NdFeO₃, J. Mag. Mag. Mater. **140–144**, 2151 (1995).

[45] K. N. R. Taylor and M. I. Darby, *Physics of Rare Earth Solids* (Chapman and Hall, London, 1972).

[46] E. Bauer and M. Rotter, Magnetism of complex metallic alloys: crystalline electric field effects, in *Properties And Applications Of Complex Intermetallics* (World Scientific, Singapore, 2010), pp. 183–248.

[47] These results are similar to those taken on SEQUOIA, Figs. 2(a) and (b), but with a much better resolution.

[48] T. Nakajima, A. Suno, S. Mitsuda, N. Terada, S. Kimura, K. Kaneko, and H. Yamauchi, Magnons and electromagnons in a spin-lattice-coupled frustrated magnet CuFeO₂ as seen via inelastic neutron scattering, Phys. Rev. B **84**, 184401 (2011).

[49] S. Hayashida, M. Soda, S. Itoh, T. Yokoo, K. Ohgushi, D. Kawana, H. M. Rønnow, and T. Masuda, Magnetic model in multiferroic NdFe₃(BO₃)₄ investigated by inelastic neutron scattering, Phys. Rev. B **92**, 054402 (2015).

[50] I. V. Golosovsky, A. K. Ovsyanikov, D. N. Aristov, P. G. Matveeva, A. A. Mukhin, M. Boehm, L. P. Regnault, and L. N. Bezmaternykh, Spin-wave dynamics and exchange interactions in multiferroic NdFe₃(BO₃)₄ explored by inelastic neutron scattering, J. Magn. Magn. Mater. **451**, 443 (2017).

[51] Y. V. Tymoshenko, Y. A. Onykiienko, T. Müller, R. Thomale, S. Rachel, A. S. Cameron, P. Y. Portnichenko, D. V. Efremov, V. Tsurkan, D. L. Abernathy, J. Ollivier, A. Schneidewind, A. Piovano, V. Felea, A. Loidl, and D. S. Inosov, Pseudo-Goldstone Magnons in the Frustrated $S = 3/2$ Heisenberg Helimagnet ZnCr₂Se₄ with a Pyrochlore Magnetic sublattice, Phys. Rev. X **7**, 041049 (2017).

[52] T. Pyttlik and K. W. Becker, Explanation of the Cu spin-wave excitation gap in Nd₂CuO₄, Eur. Phys. J. B **3**, 333 (1998).

[53] A. J. Princep, R. A. Ewings, S. Ward, S. Tóth, C. Dubs, D. Prabhakaran, and A. T. Boothroyd, The full magnon spectrum of yttrium iron garnet, npj Quant. Mater. **2**, 63 (2017).

[54] K. P. Belov, A. K. Zvezdin, A. M. Kadomtzeva, and P. Z. Levitin, *Orientational Transitions in the Rare-Earth Magnets* (Nauka, Moscow, 1979), in Russian.

[55] K. P. Belov, A. K. Zvezdin, A. M. Kadomtseva, and I. B. Krynetskiĭ, Zh. Eksp. Teor. Fiz. **67**, 1974 (1974) [New orientational transitions induced in orthoferrites by an external field, Sov. Phys.-JETP **40**, 980 (1975)].

[56] K. P. Belov, A. K. Zvezdin, and A. A. Mukhin, Zh. Eksp. Teor. Fiz. **76**, 1100 (1979) [Magnetic phase transitions in terbium orthoferrite, Sov. Phys. JETP **49**, 557 (1979)].

[57] Ya. B. Bazaliy, L. T. Tsymbal, G. N. Kakazei, A. I. Izotov, and P. E. Wigen, Spin-reorientation in $ErFeO_3$: Zero-field transitions, three-dimensional phase diagram, and anisotropy of erbium magnetism, Phys. Rev. B **69**, 104429 (2004).

[58] L. T. Tsymbal, Ya. B. Bazaliy, V. N. Derkachenko, V. I. Kamenev, G. N. Kakazei, F. J. Palomares, and P. E. Wigen, Magnetic and structural properties of spin-reorientation transitions in orthoferrites, J. Appl. Phys. **101**, 123919 (2007).

[59] K. W. H. Stevens, Matrix elements and operator equivalents connected with the magnetic properties of rare earth ions, Proc. Phys. Soc. A **65**, 209 (1952).

[60] M. T. Hutchings, Point-charge calculations of energy levels of magnetic ions in crystalline electric fields, Solid State Phys. **16**, 227 (1964).

[61] K. P. Belov, A. K. Zvezdin, A. M. Kadomtseva, and R. Z. Levitin, Spin-reorientation transitions in rare-earth magnets, Sov. Phys. Usp. **19**, 574 (1976).

[62] We would like to emphasize that the real anisotropy constants K_a and K_c have no significant T-dependencies in the considered temperature range $T \approx T_{SR}$, whereas only our new effective K'_a and K'_c, which take into account Fe-Yb interactions, are changing with temperature.

[63] Angles θ and ϕ are defined with respect to the a and b axes, respectively. See Ref. [19] for details of the notations.

[64] Details of the influence of the CEF term on the $J = 7/2$ multiplet of Yb^{3+} are discussed in Ref. [23].

[65] J. B. Torrance and M. Tinkham, Excitation of multiple-magnon bound states in $CoCl_2 \cdot 2H_2O$, Phys. Rev. **187**, 595 (1969).

[66] J. B. Torrance and M. Tinkham, Magnon bound states in anisotropic linear chains, Phys. Rev. **187**, 587 (1969).

[67] Hans C. Fogedby, Magnetic excitation spectrum of $CoCl_2 \cdot 2H_2O$, Phys. Rev. B **10**, 4000 (1974).

[68] T. Schneider and E. Stoll, Magnetic field effects in the spin dynamics of ferro- and antiferromagnetic Ising-type chains with $S = 1/2$, Phys. Rev. B **26**, 3846 (1982).

[69] R. Orbach, Linear antiferromagnetic chain with anisotropic coupling, Phys. Rev. **112**, 309 (1958).

[70] T. Schneider and E. Stoll, Excitation spectrum of the ferromagnetic Ising-Heisenberg chain at zero field, Phys. Rev. B **25**, 4721 (1982).

[71] Sam T. Carr and Alexei M. Tsvelik, Spectrum and Correlation Functions of a Quasi-One-Dimensional Quantum Ising Model, Phys. Rev. Lett. **90**, 177206 (2003).

[72] R. Coldea, D. A. Tennant, E. M. Wheeler, E. Wawrzynska, D. Prabhakaran, M. Telling, K. Habicht, and K. Kiefer P. Smeibidl, Quantum criticality in an ising chain: Experimental evidence for emergent E8 symmetry, Science **327**, 177 (2010).

[73] Due to much higher background of the CNCS setup with a cryomagnet we were not able to observe both, two-magnon bound state, and two-magnon continuum, in the low-T spectra.

[74] Due to a strong anisotropy of magnetic properties of $YbFeO_3$ we were not able to perform INS measurements for **H** ∥ [010] in field $H > 2$ T, because of the strong torque effect. Later, a special sample holder was constructed and used for the experiments with **H** ∥ [001].

[75] I. A. Zaliznyak, H. Woo, T. G. Perring, C. L. Broholm, C. D. Frost, and H. Takagi, Spinons in the Strongly Correlated Copper Oxide Chains in $SrCuO_2$, Phys. Rev. Lett. **93**, 087202 (2004).

[76] L. S. Wu, W. J. Gannon, I. A. Zaliznyak, A. M. Tsvelik, M. Brockmann, J.-S. Caux, M. S. Kim, Y. Qiu, J. R. D. Copley, G. Ehlers, A. Podlesnyak, and M. C. Aronson, Orbital-exchange and fractional quantum number excitations in an f-electron metal, Yb_2Pt_2Pb, Science **352**, 1206 (2016).

[77] P Thalmeier, Low-energy Nd spin waves in noncollinear Nd_2CuO_4, Physica C: Supercond. **266**, 89 (1996).

[78] W. Henggeler, T. Chattopadhyay, P. Thalmeier, P. Vorderwisch, and A. Furrer, Spin wave excitations of Nd in Nd_2CuO_4, Europhys. Lett. **34**, 537 (1996).

[79] X. Fabreges, I. Mirebeau, P. Bonville, S. Petit, G. Lebras-Jasmin, A. Forget, G. André, and S. Pailhes, Magnetic order in $YbMnO_3$ studied by neutron diffraction and Mössbauer spectroscopy, Phys. Rev. B **78**, 214422 (2008).